Electronic Supplementary Information for

Au_3-to-Ag_3 Coordinate-Covalent Bonding and Other Supramolecular Interactions with Covalent Bonding Strength

Zhou Lu,[†a] Bhaskar Chilukuri,[†ab] Chi Yang,[†*ac] Abdel-Monem M. Rawashdeh,[ad] Ravi K. Arvapally,[a] Sammer M. Tekarli,[ae] Xiaoping Wang,[f] Christian T. Cardenas,[a] Thomas R. Cundari *[a] and Mohammad A. Omary *[a]

[a] Department of Chemistry, University of North Texas, 1155 Union Circle #305070, Denton, Texas 76203, United States

[b] Department of Chemistry, Washington State University, Pullman, Washington 99164, United States

[c] Center for Materials Research, Norfolk State University, Norfolk, Virginia 23504, United States

[d] Department of Chemistry, Yarmouk University, Irbid 21163, Jordan

[e] Department of Chemistry, Collin College, Frisco, Texas 75035, United States

[f] Neutron Scattering Division, Oak Ridge National Laboratory, Oak Ridge, Tennessee 37831-6475, United States

[†] Z.L., B.C., and C.Y. have contributed equally to this work (co-1st authors).

Corresponding authors: *M.A.O.: omary@unt.edu.; *T.R.C.: t@unt.edu; *C.Y.: chi.yang@unt.edu

EXPERIMENTAL SECTION

Gold(tetrahydrothiophene)chloride [Au(THT)Cl], [Ag(μ-Tz-(n-C_3F_7)$_2$)]$_3$, and [Ag(μ-Pz-(CF_3)$_2$)]$_3$ were synthesized following the literature methods without modification.[1,2] Synthesis of [Au(μ-Pz-(i-C_3H_7)$_2$)]$_3$ was modified based on reported methods.[3] Other chemicals were used as received without further treatment. Solution-state and solid-state diffuse reflectance UV-Vis measurements were measured on Perkin-Elmer Lambda 900 UV/Vis/NIR spectrometer. ^{1}H and ^{19}F NMR spectra were recorded by a Varian 400 MHz spectrometer. Far-infrared (far-IR) and infrared (IR) spectra were recorded using a Nicolet 6700 analytical FTIR spectrometer equipped with a Smart Orbit high-performance diamond single bounce accessory for attenuated total reflectance measurements.

Synthesis of *cyclo*-trimer gold(I) 3,5-diisopropylpyrazolate [Au(μ-Pz-(i-C_3H_7)$_2$)]$_3$

To the 2 mL THF solution of fresh 3,5-diisopropylpyrazole (47 mg, 0.31 mmol), 3 mL THF solution of Au(THT)Cl (100 mg, 0.31 mmol) was added to afford clear colorless solution. After stirring for 5 minutes, 18 mg (0.31 mmol) potassium hydroxide dissolved in 1 mL of dry MeOH is added dropwise to the stirring solution. The resulting mixture is allowed to continue stirring for another one hour, after which the solvent is then evaporated to dryness under reduced pressure. The remaining solid is dissolved in a minimum amount of THF and participated by adding excess acetonitrile. The white powder (83 mg, 76% yield based on Au(THT)Cl) is obtained by filtration and drying under vacuum. ^{1}H NMR (400 MHz, $CDCl_3$): δ (ppm) = 6.13 (s, 1.00, 4*H* of Pz), 3.12 (sept, 2.02, -C*H* of i-C_3H_7), 1.34 (d, 11.99, -C*H*$_3$ of i-C_3H_7). Elemental analyses for $Au_3N_6C_{27}H_{45}$, calcd (%): C 31.04, N 8.05, H 4.34; found (%): C 31.19, N 8.07, H 3.94.

Synthesis of stacked *cyclo*-trimer [Au(μ-Pz-(i-C_3H_7)$_2$)]$_3$•[Ag(μ-Tz-(n-C_3F_7)$_2$)]$_3$ (**1**)

A solution of [Ag(μ-Tz-(n-C_3F_7)$_2$)]$_3$ (30 mg, 0.02 mmol) in hot chloroform (20 mL) was added to a solution of [Au(μ-Pz-(i-C_3H_7)$_2$)]$_3$ (21 mg, 0.02 mmol) in hot benzene (20 mL), and the resulting mixture was heated under argon for 3 h. After evaporation of the solvent, the residue (14 mg, 27% yield) was re-dissolved in a small amount of benzene and put for slow evaporation under nitrogen. Colorless prisms suitable for X-ray crystal structure analysis were obtained after one week, which were wrapped in paraffin oil and submitted for data collection at 100 K. ^{1}H NMR (400 MHz, d_6-DMSO): δ (ppm) = 6.35 (s, 3.00, 4*H* of Pz), 3.04 (sept, 6.02, -C*H* of i-C_3H_7), 1.30 (d, 32.86, -C*H*$_3$ of i-C_3H_7). ^{19}F NMR (400 MHz, d_6-DMSO): δ (ppm) = 79.95 (t, 18.00, -C*F*$_3$), 109.87 (m, 11.90, -CF_2C*F*$_2$$CF_3$), 126.66 (d, 11.90, -C*F*$_2$$CF_2CF_3$). FT-IR ($\nu$/cm^{-1}): 2956(w), 2867(w), 1972(m), 1525(w), 1454(w), 1344(s), 1211(s), 1176(m), 1116(s), 1018(s), 929(s), 883(s), 750(s), 669(m). Elemental analyses for $Au_3Ag_3N_{15}C_{51}H_{45}F_{42}$, calcd (%): C 23.74, N 8.14, H 1.76; found (%): C 23.78, N 7.52, H 1.82.

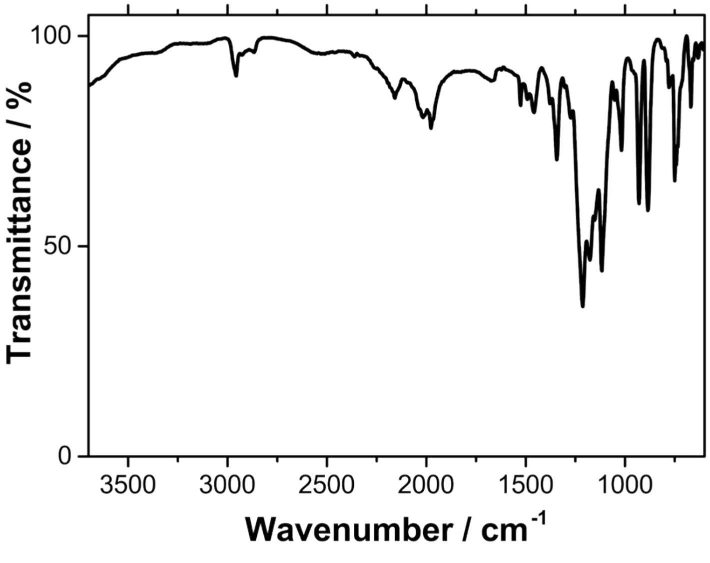

Figure S1. Infrared spectrum of neat solid powder of **1** in the mid-IR region.

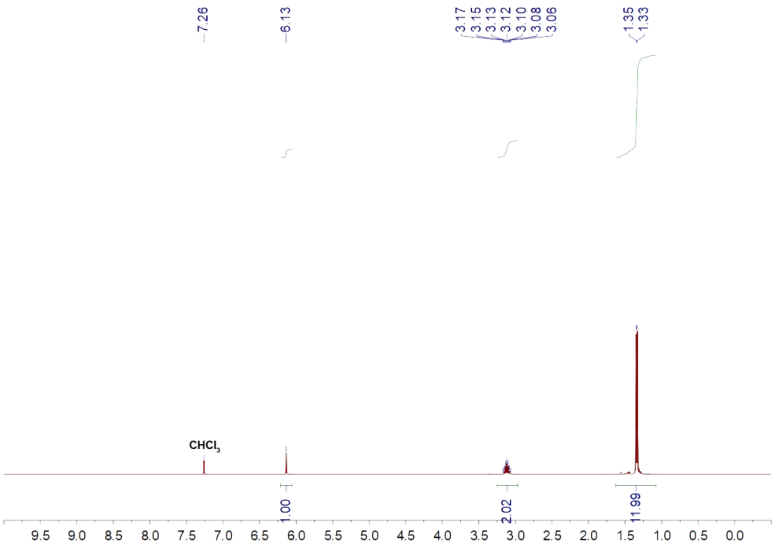

Figure S2. ^{1}H-NMR spectrum of [Au(μ-Pz-(i-C_3H_7)$_2$)]$_3$.

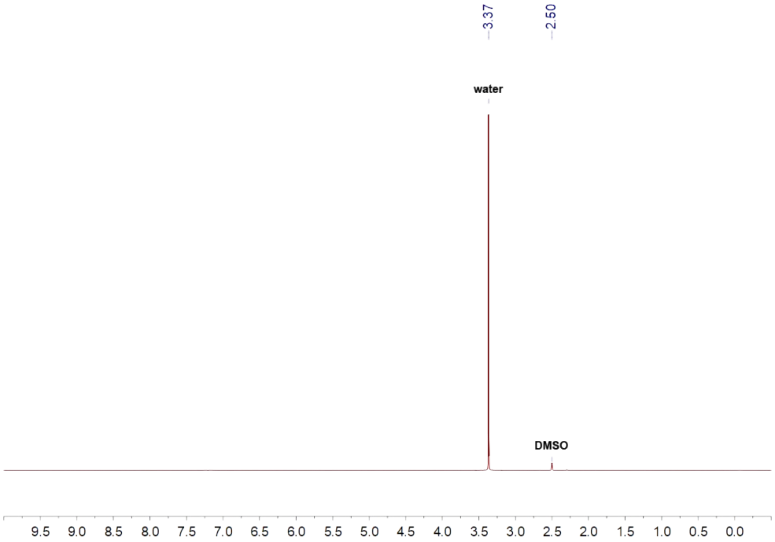

Figure S3. ^{1}H-NMR spectrum of [Ag(μ-Tz-(n-C_3F_7)$_2$)]$_3$.

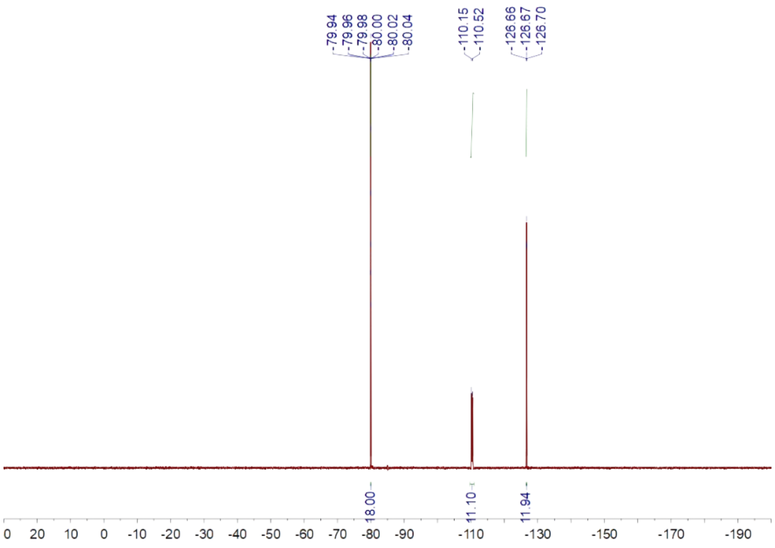

Figure S4. ^{19}F-NMR spectrum of [Ag(μ-Tz-(n-C_3F_7)$_2$)]$_3$.

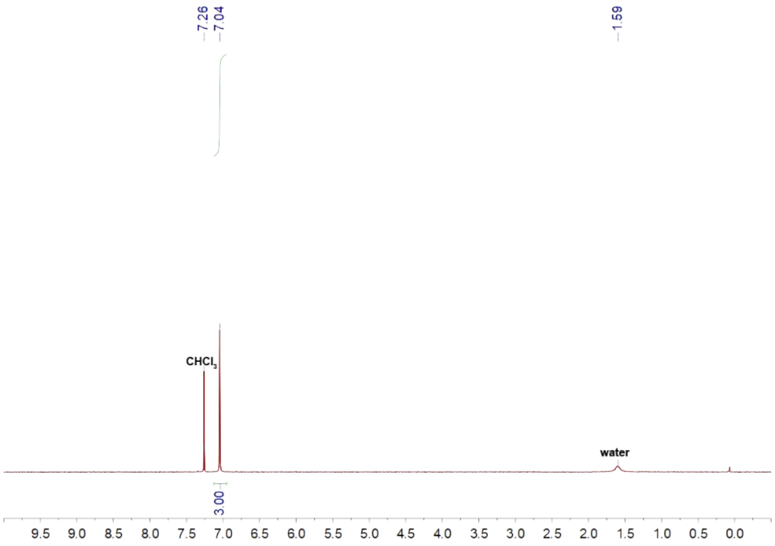

Figure S5. ^{1}H-NMR spectrum of [Ag(μ-Pz-(CF_3)$_2$)]$_3$.

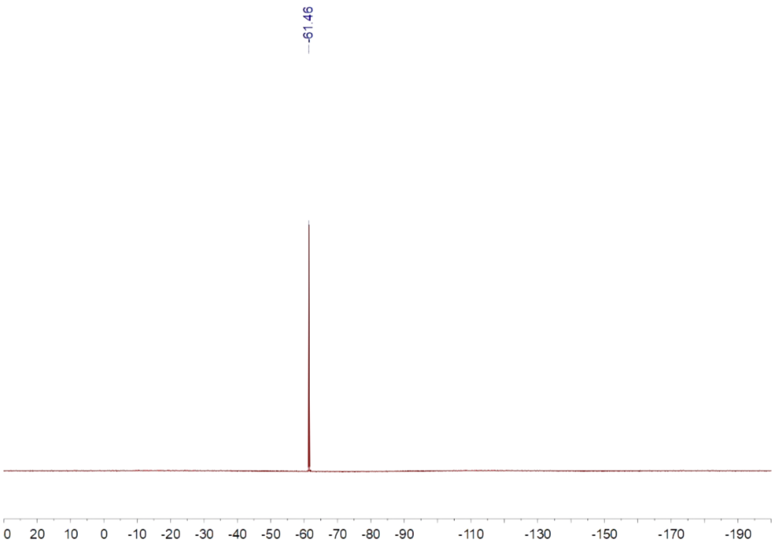

Figure S6. ^{19}F-NMR spectrum of [Ag(μ-Pz-(CF$_3$)$_2$)]$_3$.

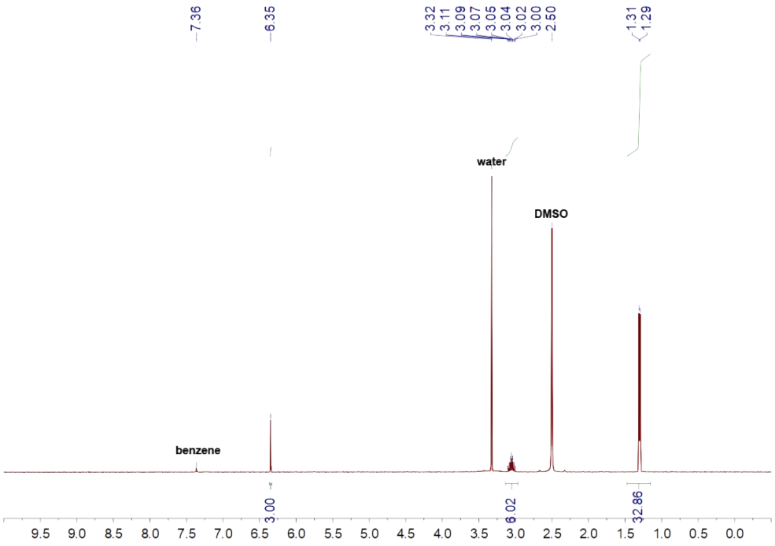

Figure S7. ^{1}H-NMR spectrum of **1**.

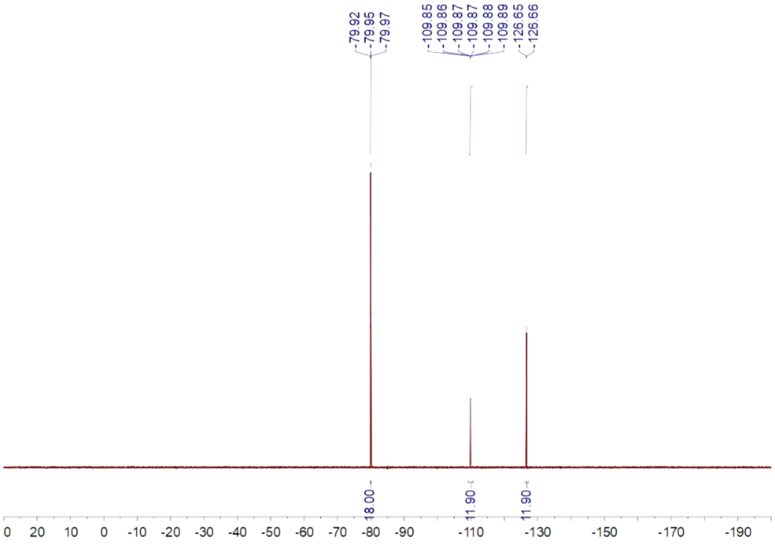

Figure S8. ^{19}F-NMR spectrum of **1**.

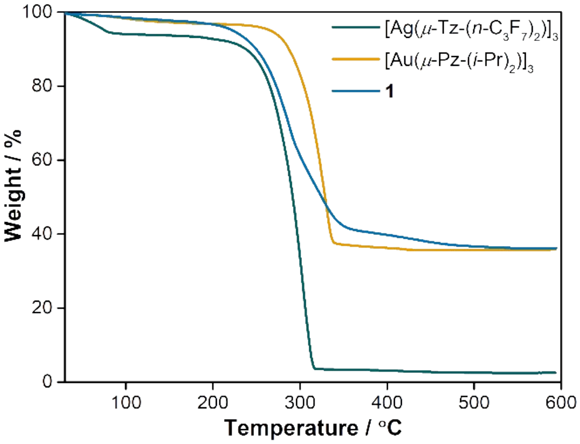

Figure S9. Thermogravimetric analysis (TGA) curves of [Ag(μ-Tz-(n-C_3F_7)$_2$)]$_3$, [Au(μ-Pz-(i-C_3H_7)$_2$)]$_3$, and **1**.

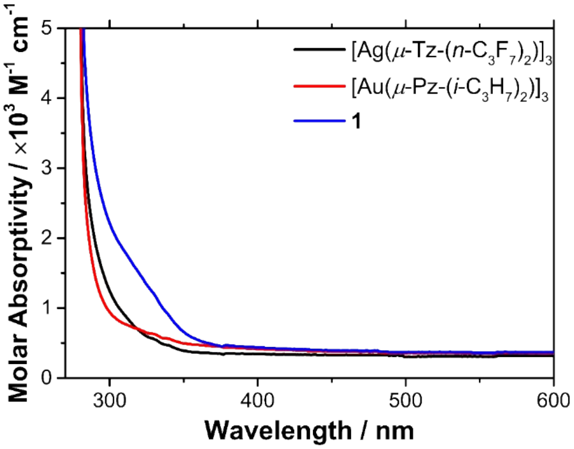

Figure S10. Solution-state UV-vis spectra for $[Ag(\mu\text{-Tz-}(n\text{-}C_3F_7)_2)]_3$, $[Au(\mu\text{-Pz-}(i\text{-}C_3H_7)_2)]_3$, and **1** in benzene.

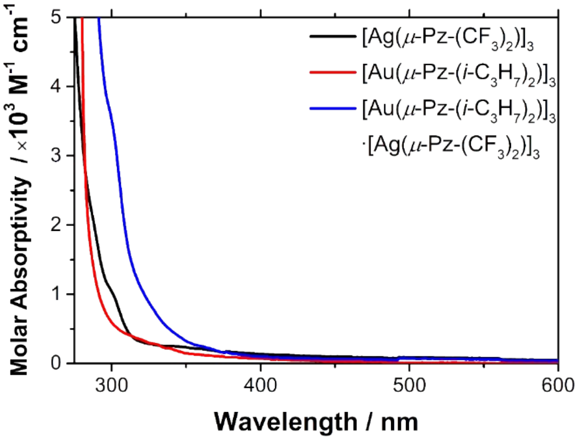

Figure S11. Solution-state UV-vis spectra for $[Ag(\mu\text{-Pz-}(CF_3)_2)]_3$, $[Au(\mu\text{-Pz-}(i\text{-}C_3H_7)_2)]_3$, and $[Au(\mu\text{-Pz-}(i\text{-}C_3H_7)_2)]_3\cdot[Ag(\mu\text{-Pz-}(CF_3)_2)]_3$ in benzene.

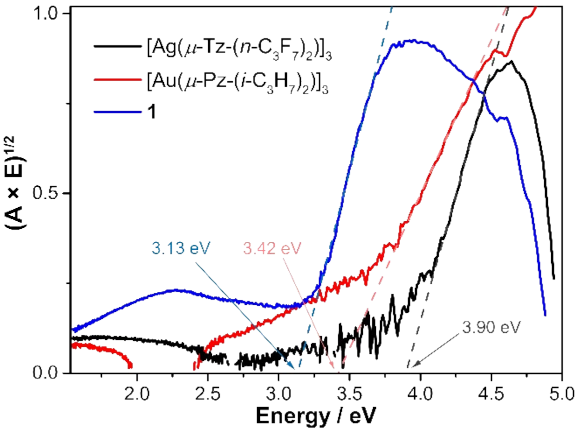

Figure S12. Solid-state diffuse reflectance spectra of $[Ag(\mu\text{-}Tz\text{-}(n\text{-}C_3F_7)_2)]_3$, $[Au(\mu\text{-}Pz\text{-}(i\text{-}C_3H_7)_2)]_3$, and **1** (where A is absorbance).

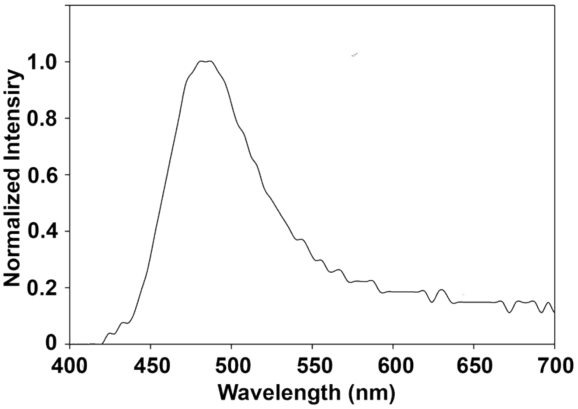

Figure S13. Solid-state emission spectrum of **1**.

CRYSTALLOGRAPHIC STUDIES

X-ray Structure Determination. A colorless crystal, approximate dimensions 0.39 mm × 0.26 mm × 0.14 mm, was used for the X-ray crystallographic analyses. Frame data were collected on a Bruker SMART APEX II CCD area detector system equipped with a graphite monochromator and a Mo Kα fine-focus sealed tube (λ = 0.71073 Å). The frame data were integrated with the APEX2 software package[4a] using a narrow-frame integration algorithm and final cell refinements were done using SAINT.[4b] Data were corrected for absorption effects using the multi-scan technique (SADABS).[4c] The structure was solved in space group $R3m$ and refinement, graphic and generation of publication materials were performed with the ShelxL appended in OLEX2 1.2 program package.[4d-e] Detailed structure refinement information was enclosed in the CIF file. CCDC no. 1899711. The data can be obtained free of charge from The Cambridge Crystallographic Data Centre https://www.ccdc.cam.ac.uk.

Table S1. Crystal data and structure refinement for [Au(μ-Pz-(i-C_3H_7)$_2$)]$_3$•[Ag(μ-Tz-(n-C_3F_7)$_2$)]$_3$ (1).

CCDC No.	1899711
Empirical formula	C57 H51 Ag3 Au3 F42 N15
Formula weight	2658.58
Temperature	100(2) K
Wavelength	0.71073 Å
Crystal system	Trigonal
Space group	$R\,3\,m$
Unit cell dimensions	a = 25.7253(8) Å, α= 90°.
	b = 25.7253(8) Å, β= 90°.
	c = 10.2918(6) Å, γ = 120°.
Volume	5898.5(5) Å^3
Z	3
Density (calculated)	2.245 Mg/m^3
Absorption coefficient	6.455 mm^{-1}
F(000)	3762
Crystal size	0.39 × 0.26 × 0.14 mm^3
2 Theta range for data collection	3.166 to 51.416°
Index ranges	$-31 \le h \le 31$, $-31 \le k \le 31$, $-12 \le l \le 12$
Reflections collected	18891
Independent reflections	2661 [R_{int} = 0.0305, R_{sigma} = 0.0390]
Completeness to theta = 25.71°	99.6 %
Absorption correction	Numerical
Refinement method	Full-matrix least-squares on F^2
Data / restraints / parameters	2661 / 117 / 213
Goodness-of-fit on F^2	1.047
Final R indices [I>2sigma(I)]	R_1 = 0.0432, wR_2 = 0.1049
R indices (all data)	R_1 = 0.0459, wR_2 = 0.1069
Flack parameter	0.010(17)
Largest diff. peak and hole	1.54 and -4.08 e.Å^{-3}

$R_1 = \sum||F_o| - |F_c||/\sum|F_o|$. $wR_2 = \{[\sum w(F_o^2-F_c^2)^2]/\sum[w(F_o^2)^2]\}^{1/2}$; $w = 1/[\sigma^2(F_o^2) + (aP)^2 + bP]$, where $P = [\max(F_o^2,0) + 2F_c^2]/3$ for all data.

Table S2. Selected bond length (Å) and angle (°) of $[\mathrm{Au}(\mu\text{-Pz-}(i\text{-}C_3H_7)_2)]_3\bullet[\mathrm{Ag}(\mu\text{-Tz-}(n\text{-}C_3F_7)_2)]_3$ (1).

Ag(1)-N(1)	2.104(16)	Au(1)-Au(1)#3	3.3578(18)
Ag(1)-N(1)#1	2.104(16)	Au(1)-Au(1)#1	1.6770(19)
Ag(1)-Au(1)	3.0462(18)	Au(1)-Au(1)#2	2.189(2)
Ag(1)-Au(1)#1	3.0462(18)	Au(1)-Au(1)#4	3.3578(18)
N(1)-N(1)#2	1.39(4)	Au(1)-N(3)	1.97(3)
N(1)-Ag(1)-N(1)#1	165.1(7)	Ag(1)-Au(1)-Au(1)#4	96.27(3)
N(1)#1-Ag(1)-Au(1)	113.4(3)	Au(1)#1-Au(1)-Ag(1)	74.02(2)
N(1)-Ag(1)-Au(1)#1	113.4(3)	Au(1)#2-Au(1)-Ag(1)	102.37(3)
N(1)-Ag(1)-Au(1)	81.4(3)	Au(1)#2-Au(1)-Au(1)#3	85.63(3)
N(1)#1-Ag(1)-Au(1)#1	81.4(3)	Au(1)#1-Au(1)-Au(1)#4	94.37(3)
Au(1)-Ag(1)-Au(1)#1	31.96(4)	Au(1)#3-Au(1)-Au(1)#4	60
N(1)#2-N(1)-Ag(1)	120.0(5)	Au(1)#2-Au(1)-Au(1)#4	25.63(3)
C(1)-N(1)-Ag(1)	134.4(17)	Au(1)#1-Au(1)-Au(1)#2	120
Ag(1)-Au(1)-Au(1)#3	79.79(3)	N(3)-Au(1)-Au(1)#2	143.8(10)
Au(1)#1-Au(1)-Au(1)#3	34.37(3)	N(3)-Au(1)-Au(1)#4	118.2(10)
Au(1)#1-Au(1)-N(3)	23.9(10)	N(4)-N(3)-Au(1)	124(3)
N(3)-Au(1)-Ag(1)	75.3(8)	C(5)-N(3)-Au(1)	128(2)
N(3)-Au(1)-Au(1)#3	58.2(10)		

Symmetry transformations used to generate equivalent atoms:

#1 -x+y,y,z #2 -y,-x,z #3 -y,x-y,z #4 -x+y,-x,z #5 x,x-y,z

Scheme S1. Molecular structures of reference complexes 4a and 2a in the literature.

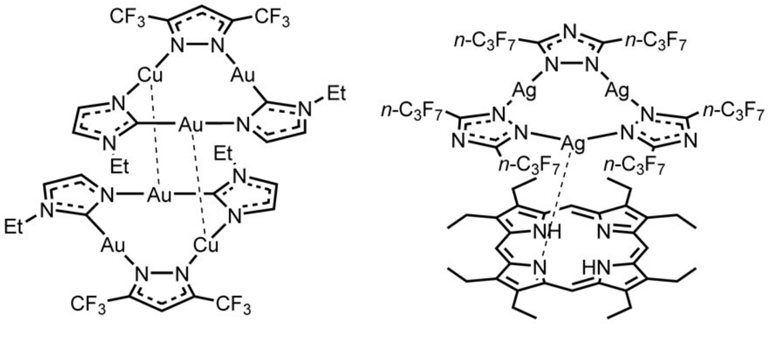

4a in *Proc. Natl. Acad. Sci. U.S.A.* **2017**, *114*, E5042–E5051.

2a in *Angew. Chem., Int. Ed.* **2015**, *54*, 4842–4846.

COMPUTATIONAL METHODOLOGY

Solid State Computational Methods. Solid state calculations are performed with density functional theory (DFT) using the Vienna Ab-initio Simulation Package (VASP) which uses plane wave basis sets and Projector Augmented Wave (PAW) methods for treating the interaction among the ions and valence electrons.[5] The Kohn-Sham single electron wave functions are expanded by a series of plane waves with respective cutoff energies. The generalized gradient approximation (GGA) functional of Perdew, Burke and Ernzerhof (PBE)[6] was used for all the calculations. Although pure-DFT functionals have well known limitations in describing localized states in wide band gap semiconductors and underestimates band gaps, the trend of calculated properties remains consistent with hybrid-DFT methods.[7] Considering the size of the unit cell lattice parameters and the number of atoms in each unit cell, the electronic wave functions are sampled in the first Brillouin zone on a k-point mesh size of 1 × 1 × 3 using the Monkhorst-Pack method.[8] The cut off energies used for the Ag/Au, Au, Ag trimers were 400, 750, 750 eVs, respectively, as determined from corresponding energy convergence plots. Charge densities are viewed using Molekel.[9]

Molecular Modeling Methods. Geometry optimizations and single point calculations were performed using the Gaussian 16 program[10], with the level of B97D3 functional[11], with built-in Grimme dispersion correction (D3) and Becke-Johnson damping functions (BJ), and the CEP-31G(d) valence basis set[12], where (d) signifies addition of a d-polarization function to main group elements. No imaginary frequencies were found to assure optimized structures were minima. Potential energy surface (PES) scans were conducted on the B97D3 and M06[13] optimized structure **1** with co-crystallized benzene and separating Au_3 and [Ag_3•benzene] fragments into two parts, with the functionals of B97D3, M06, and M06-D3 along with the CEP-31G(d) pseudopotential/valence basis sets. The monomers of Au_3 and [Ag_3•benzene] remained the same as those in the optimized dimer-of-trimer of Au_3/Ag_3 stacking; the only variable in the scan calculations was the separation distance between centroids of Au_3 and Ag_3 along the z-axis.

Wavefunction analysis were performed using the B97D3 functional and triple-zeta all-electron relativistic basis sets, which is Sapporo-DKH3-TZP-2012 for metal atoms and cc-pVTZ-DK for light atoms.[14] Reduced density gradient (RDG) maps were generated by the Multiwfn 3.6 (dev) and Visual Molecular Dynamics (VMD) programs while scatter plots were visualized by gnuplot software, using wavefunction (.wfn) files produced by Gaussian.[15] RDG analysis, developed by Yang *et al.*,[16] is a useful tool to understand weak interactions and spatial distribution of non-covalent interactions (Equation S1). The second largest eigenvalue of the electron density Hessian matrix of low-density regions and the value of product of electron density $(r) \times \text{sign}(\lambda_2)$ are calculated to determine the nature of attractive or repulsive interactions. As a consequence, if the value of $\text{sign}(\lambda_2) \times r$ is *ca.* zero, van del Waals forces, like hydrogen bonding, can be characterized, while for a positive value, steric repulsion would be expected in the region.

$$RDG(r) = \frac{1}{2(3\pi^2)^{1/3}} \times \frac{|\nabla\rho(r)|}{\rho(r)^{4/3}} \qquad \text{(S1)}$$

Energy decomposition analysis (EDA)[17] was performed by the ADF2018[18] program package. Slater type triple-zeta double-polarization basis sets (TZ2P) and no frozen core were adapted with relativistics effect considered by applying the zeroth-order regular approximation (ZORA) in the Dirac equation.[19] B3LYP functional[20] with D3-BJ dispersion correction was employed for the study of metal-metal interactions and van der Waals interactions. Developed by Ziegler *et al.*, quantitative interpretation of chemical bonds and interactions in terms of four expressions may be obtained from EDA, as depicted in Equation S2. The interaction energy (ΔE_{int}) between fragments A and B in a complex A-B is decomposed into electrostatic interaction (ΔE_{elstat}), Pauli repulsion between electrons of different fragments with the same spin multiplicity (ΔE_{Pauli}), orbital interaction (ΔE_{OrbInt}) and dispersion correction (ΔE_{disp}).

$$\Delta E_{\text{int}} = \Delta E_{\text{elstat}} + \Delta E_{\text{Pauli}} + \Delta E_{\text{OrbInt}} + \Delta E_{\text{Disp}} \qquad \text{(S2)}$$

With the EDA-NOCV (EDA-Natural orbital for chemical valence) method,[21] deformation density is quantitively partitioned into the different components of the chemical bonds that are being analyzed. The energy contribution of each bond to the total bond energy is calculated to evaluate and discuss the orbital interactions. By visualizing the deformation electronic density, the directions of electron flow could be clearly deciphered to gain insight into orbital interactions.

Binding energies and some thermodynamic chemistry parameters were calculated as well to evaluate the complexation between two different cyclic trinuclear d^{10}-metal complexes (CTCs). The computational studies were performed by Gaussian 16, with the level of theory being the B97D3 functional and CEP-31G(d) basis sets. The models we chose here were from this work, and previous work that attempted to synthesize mixed-metal complexes from CTCs. For details, refer to Table S5.

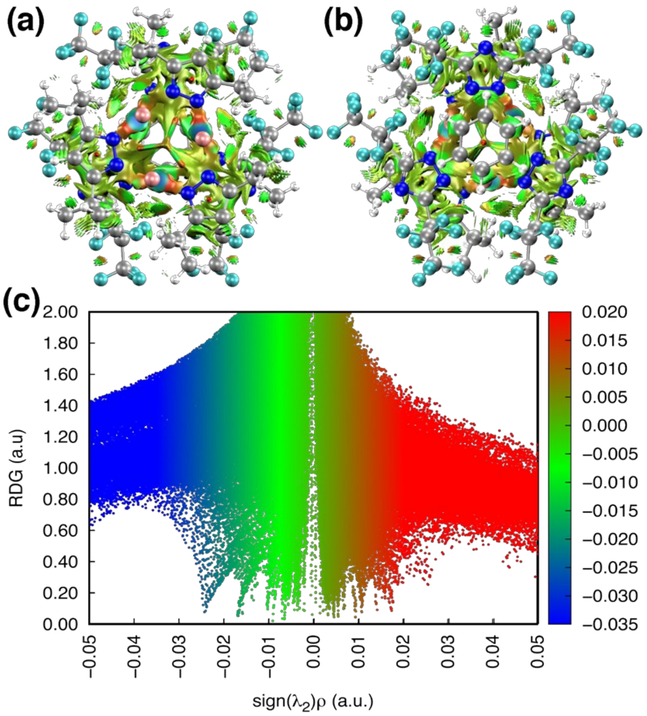

Figure S14. Reduced Density Gradient (RDG) maps of (a) Au–Ag interaction region and (b) Ag-Benzene interaction region (isosurface = 0.5 a.u.). (c) Scatter plots of RDG analysis. Blue-green-red colouring scale (from -0.035 a.u. to 0.02 a.u.) reflects attractive through repulsive interactions, for example, green regions indicating van der Waals interactions while orange/brown regions showing weak steric hindrance. The atoms are coloured light brown (Au, Ag), grey (C), blue (N), cyan (F) and white (H).

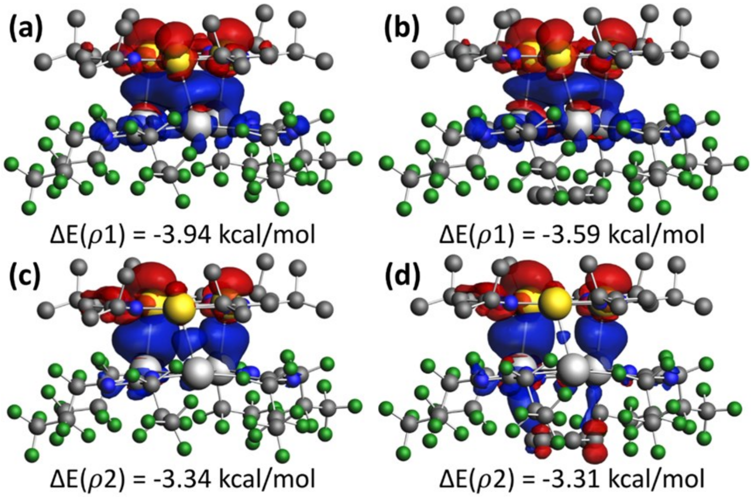

Figure S15. EDA-NOCV calculated main deformation densities ($\Delta\rho$) of $[Au(\mu\text{-Pz-}(i\text{-}C_3H_7)_2)]_3{\cdot}Ag(\mu\text{-Tz-}(n\text{-}C_3F_7)_2)]_3$ (**1**) (a,c) without benzene and (b,d) with benzene. Electrons flow from red regions to blue regions during the formation of orbital interactions. The atoms are coloured yellow (Au), light grey (Ag), dark grey (C), blue (N) and green (F). Hydrogen atoms are omitted from the figure for clarity purposes.

Table S3. Energy decomposition analysis (EDA) results of $[Ag(NH_3)_2]^+$. Fragments are decomposed of silver cation and two ammonia molecules. (unit: kcal/mol)

	$\Delta E_{\mathrm{elstat}}$	$\Delta E_{\mathrm{Pauli}}$	$\Delta E_{\mathrm{OrbInt}}$	ΔE_{Disp}	ΔE_{int}
$[Ag(NH_3)_2]^+$	-155.9 (68%)	132.9	-67.9 (30%)	-4.2 (2%)	-95.1

Symmetry-Adapted Perturbation Theory (SAPT) implemented via the program PSI4[22-26] provides a means for computing the noncovalent interaction between two molecules or fragments, and offers an instructive decomposition of the overall interaction energy into electrostatic, induction, exchange, and dispersion components. Simplest truncation of SAPT is denoted as SAPT0 to deal with large system containing over one hundred atoms. A recipe for scaled sSAPT0, simply treating the monomers at the Hartree-Fock level and appending explicit dispersion terms emerging from second-order perturbation theory to other terms inherited from a HF dimer treatment, is also presented.[27] The subscripts "elstat," "exch", "ind", and "disp" refer to electrostatics, exchange, induction, and dispersion, respectively; the total energy of SAPT0 is defined in Equation S3. The total SAPT0 and sSAPT0 interaction energy is the sum of all energy terms listed in Table S3, calculated with the def2-TZVP basis set.[28]

SAPT0
$$E_{SAPT0} = E_{elstat} + E_{exch} + E_{ind} + E_{disp} \qquad \text{(S3)}$$

Table S4. SAPT values and contribution for $[Au(\mu\text{-Pz-}(i\text{-}C_3H_7)_2)]_3$•$[Ag(\mu\text{-Tz-}(n\text{-}C_3F_7)_2)]_3$ alone and with a co-crystallized benzene molecule. (unit: kcal/mol)

	Au3•Ag3				**Au3•Ag3•Benzene**			
	SAPT0		**sSAPT0**		**SAPT0**		**sSAPT0**	
$\boldsymbol{E}$	-60.4		-59.9		-60.5		-60.0	
$\boldsymbol{E}_{\mathbf{elstat}}$	-37.6	29%	-37.6	29%	-37.4	29%	-37.4	29%
$\boldsymbol{E}_{\mathbf{exch}}$	67.8		67.8		68.0		68.0	
$\boldsymbol{E}_{\mathbf{ind}}$	-14.4	11%	-14.1	11%	-13.5	11%	-13.1	10%
$\boldsymbol{E}_{\mathbf{disp}}$	-76.1	60%	-76.0	60%	-77.6	60%	-77.5	61%
$\boldsymbol{E}_{\mathbf{ind}}$ / $\boldsymbol{E}_{\mathbf{elstat}}$		38%		38%		36%		35%

Table S5. Comparisons of binding energies and thermodynamic parameters of complexations between different CTCs. (T = 298 K, unit: kcal/mol)

Entry	Type		ΔE	ΔH	TΔS	ΔG
1		Au_3 = [Au(μ-Pz-(i-C_3H_7)$_2$)]$_3$, Ag_3 = [Ag(μ-Tz-(n-C_3F_7)$_2$)]$_3$, This work				
	i	$Au_3 + Ag_3 = Au_3Ag_3$	-62.6	-60.8	-22.2	-38.6
	monomer of (ii)	2/3 Au_3 + 1/3 Ag_3 = Au_2Ag	2.4	2.4	2.6	-0.2
	ii	4/3 Au_3 + 2/3 Ag_3 = Au_2Ag_dimer	-54.6	-52.6	-20.6	-32.1
	monomer of (iii)	1/3 Au_3 + 2/3 Ag_3 = $AuAg_2$	-1.1	-1.1	0.4	-1.5
	iii	2/3 Au_3 + 4/3 Ag_3 = $AuAg_2$_dimer	-48.4	-46.8	-19.1	-27.6
2		Au_3 = [Au(μ-Im-(N-Et))]$_3$, Cu_3 = [Cu(μ-Pz-(CF_3)$_2$)]$_3$, *Proc. Natl. Acad. Sci. U.S.A.* **2017**, *114*, E5042–E5051.[29]				
	i	$Au_3 + Cu_3 = Au_3Cu_3$	-51.4	-50.2	-20.0	-30.2
	monomer of (ii)	2/3 Au_3 + 1/3 Cu_3 = Au_2Cu	-3.4	-3.3	-0.5	-2.8
	ii	4/3 Au_3 + 2/3 Cu_3 = Au_2Cu_dimer	-49.7	-48.3	-17.7	-30.6
	monomer of (iii)	1/3 Au_3 + 2/3 Cu_3 = $AuCu_2$	-3.5	-3.5	-0.7	-2.9
	iii	2/3 Au_3 + 4/3 Cu_3 = $AuCu_2$_dimer	-45.0	-43.6	-20.0	-23.6
3		Au_3 = [Au(μ-Im-(N-Bz))]$_3$, Ag_3 = [Ag(μ-Pz-Ph_2)]$_3$, *Inorg. Chem.* **2006**, *45*, 7770–7776.[30]				
	i	$Au_3 + Ag_3 = Au_3Ag_3$	-71.5	-69.4	-23.1	-46.2
	monomer of (ii)	2/3 Au_3 + 1/3 Ag_3 = Au_2Ag	-2.1	-2.3	-1.7	-0.6
	ii	4/3 Au_3 + 2/3 Ag_3 = Au_2Ag_dimer	-67.2	-65.3	-23.0	-42.3
	monomer of (iii)	1/3 Au_3 + 2/3 Ag_3 = $AuAg_2$	-2.8	-2.9	-1.2	-1.7
	iii	2/3 Au_3 + 4/3 Ag_3 = $AuAg_2$_dimer	-81.1	-78.5	-22.5	-56.1
4		Au_3 = [Au(μ-(p-Tol)N=C(OEt))]$_3$, Ag_3 = [Ag(μ-Pz-Ph_2)]$_3$, *Inorg. Chem.* **2006**, *45*, 7770–7776;[30] *J. Am. Chem. Soc.* **2005**, *127*, 5012–5013.[31]				
	i	$Au_3 + Ag_3 = Au_3Ag_3$	-78.4	-75.4	-26.8	-48.7
	monomer of (ii)	2/3 Au_3 + 1/3 Ag_3 = Au_2Ag	-1.0	-0.9	-0.1	-0.8
	ii	4/3 Au_3 + 2/3 Ag_3 = Au_2Ag_dimer	-79.2	-75.9	-29.0	-46.9
	monomer of (iii)	1/3 Au_3 + 2/3 Ag_3 = $AuAg_2$	-1.4	-1.4	0.4	-1.8
	iii	2/3 Au_3 + 4/3 Ag_3 = $AuAg_2$_dimer	-86.9	-83.7	-28.6	-55.0

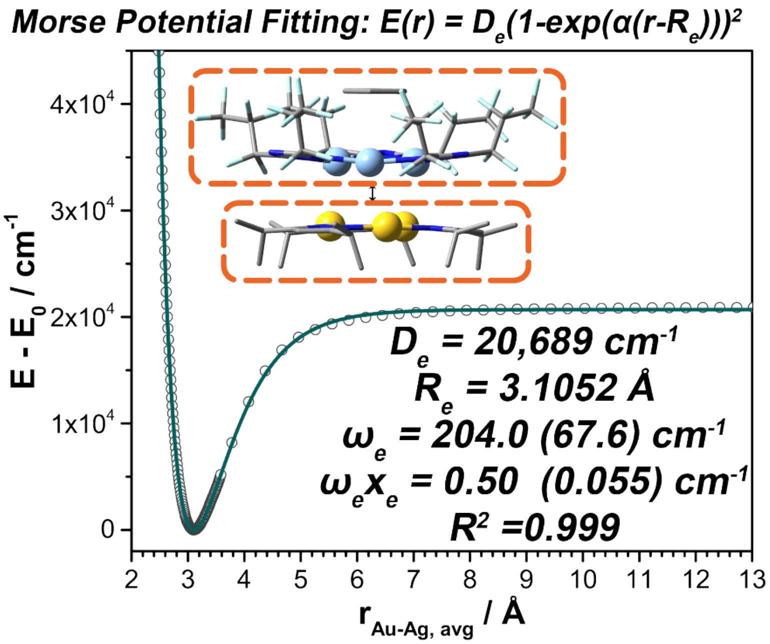

Figure S16. Potential energy surface (PES) plot upon varying the vertical intertrimer separation in the M06 fully-optimized structure of **1**•Benzene at the M06/CEP-31G(d) level of theory. The inserted illustration shows the direction of separation of the dimer-of-trimer model. Bonding and spectroscopic constants are given for ω_e and $\omega_e x_e$ values (in cm^{-1}) given based on the reduced masses of Au-Ag metal atoms versus (values in parentheses use the entire molecule for calculating the reduced masses).

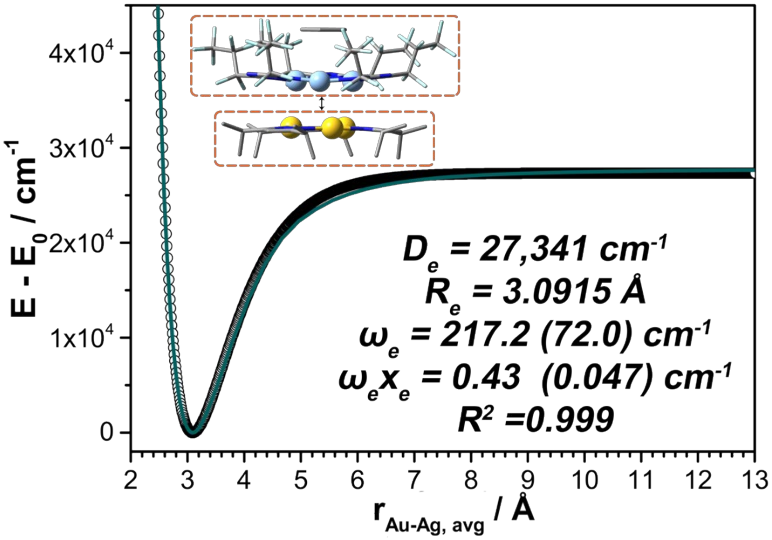

Figure S17. Potential energy surface (PES) plot upon varying the vertical intertrimer separation in the M06 fully-optimized structure of **1**•Benzene at M06-D3/CEP-31G(d) level of theory. The inserted illustration shows the direction of separation of the dimer-of-trimer model. Bonding and spectroscopic constants are given for ω_e and $\omega_e x_e$ values (in cm^{-1}) given based on the reduced masses of Au-Ag metal atoms versus (values in parentheses use the entire molecule for calculating the reduced masses).

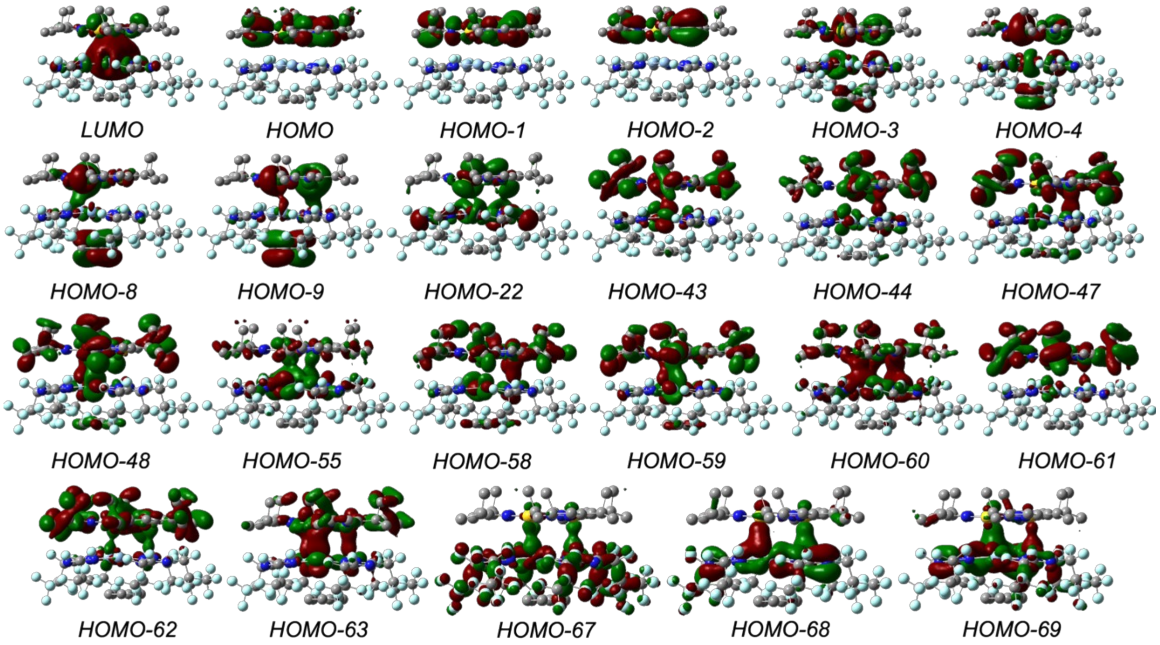

Figure S18. Kohn-Sham contours of frontier molecular orbitals with significant electron density on inter-trimer metal-metal interaction/bonding of 1 at the level of B97D3/CEP-31G(d) method. The iso-density is 0.02 a.u. for all contours.

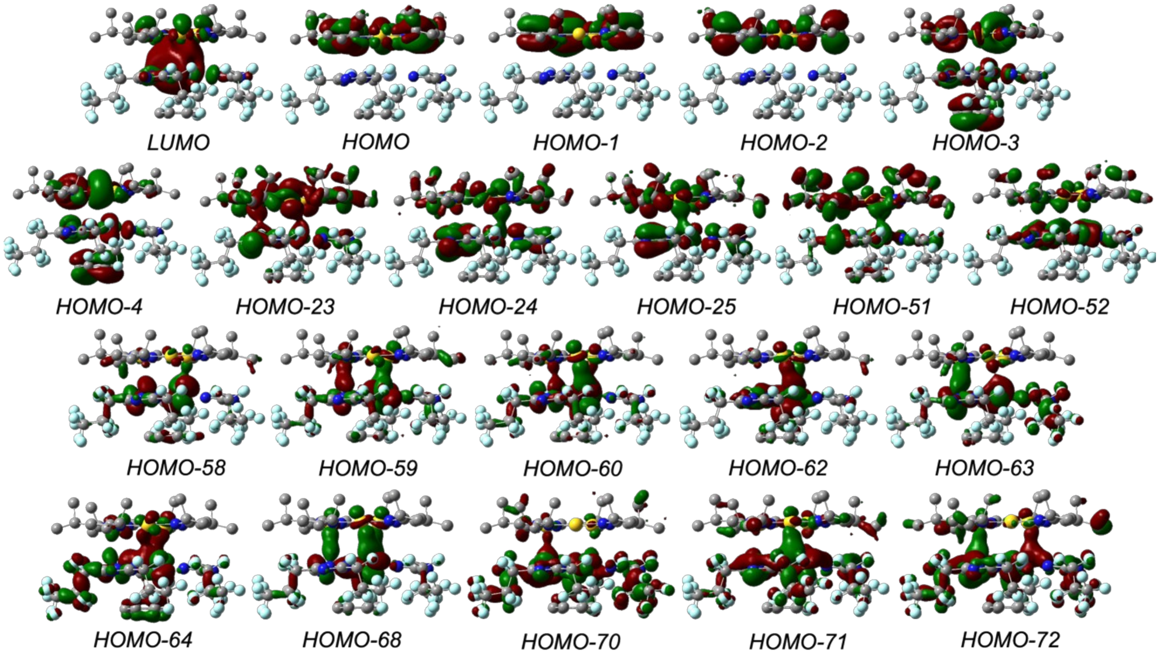

Figure S19. Kohn-Sham contours of frontier molecular orbitals with significant electron density on inter-trimer metal-metal interaction/bonding of 1 at the level of M06/CEP-31G(d) method. The iso-density is 0.02 a.u. for all contours.

Table S6. PW-DFT calculated Fermi energies (E_f) and total energies of the D•A materials at respective distances between the trimers. *Experimental distance.

Distance (Å)	E_f (eV)	E-Total (eV)
2.7	-5.3443	-908.84
2.8	-5.3436	-909.28
2.9	-5.3126	-909.73
3.0*	-5.2820	-910.03
3.1	-5.2595	-910.10
3.2	-5.2291	-910.12
3.3	-5.1733	-910.06
3.4	-5.1570	-910.00
3.6	-5.0713	-909.45

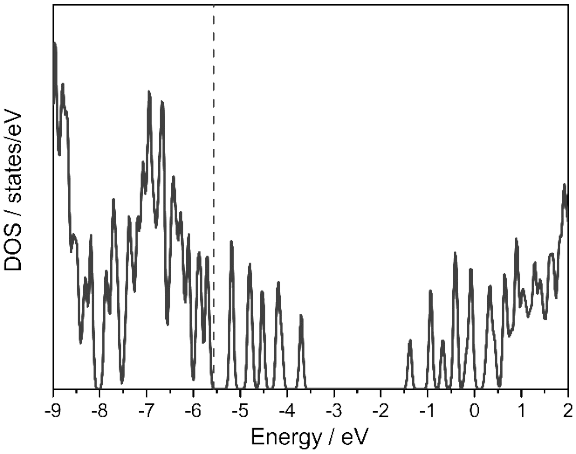

Figure S20. Calculated density of states (DOS) of D·A in the other disordering orientation. The dotted line denotes the Fermi energy (E_{Fermi} = -5.6 eV).

In the Solid-State Modeling Section, we calculated density of states (DOS) of 1 by omitting one set disordering of Au_3 trimer. To eliminate the influence of disordering, DOS of the other disordering orientation was calculated and both DOS distribution indicated that the disordering Au_3 trimer would not influence the charge-transfer property and our conclusion in the main text.

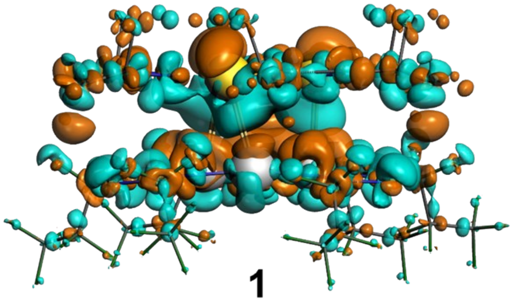

1

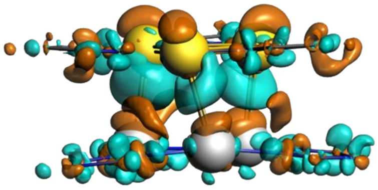

$[\mathrm{Au}(\mu\text{-Pz})]_3\bullet[\mathrm{Ag}(\mu\text{-Tz})]_3$

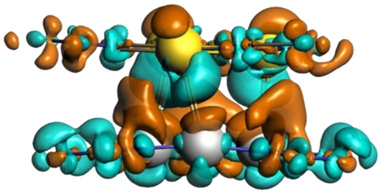

$[\mathrm{Au}(\mu\text{-Im})]_3\bullet[\mathrm{Ag}(\mu\text{-Tz})]_3$

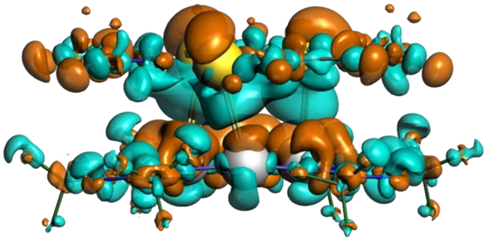

$[\mathrm{Au}(\mu\text{-Pz}(\mathrm{Me})_2)]_3\bullet[\mathrm{Ag}(\mu\text{-Tz}(\mathrm{CF}_3)_2)]_3$

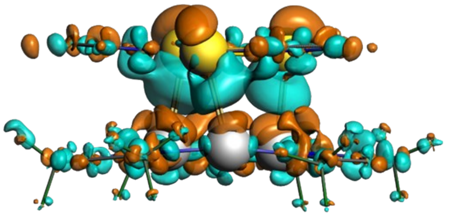

$[\mathrm{Au}(\mu\text{-Pz}(\mathrm{Me})_2)]_3\bullet[\mathrm{Ag}(\mu\text{-Pz}(\mathrm{CF}_3)_2)]_3$

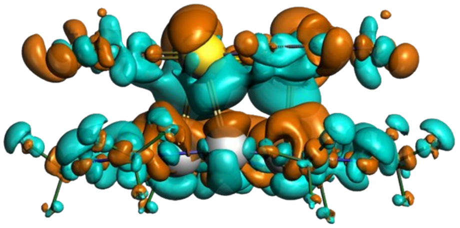

$[\mathrm{Au}(\mu\text{-Im}(\mathrm{Me})_2)]_3\bullet[\mathrm{Ag}(\mu\text{-Tz}(\mathrm{CF}_3)_2)]_3$

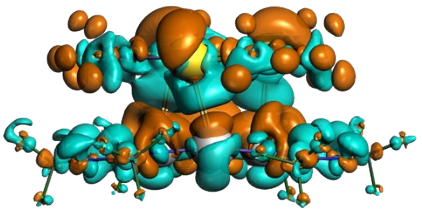

$[\mathrm{Au}(\mu\text{-Cb}(\mathrm{Me})_2)]_3\bullet[\mathrm{Ag}(\mu\text{-Tz}(\mathrm{CF}_3)_2)]_3$

Figure S21. Charge density difference (CDD) maps (isovalue = 0.0005 a.u.) for charge-transfer dimer-of-trimers (DOT). The upper fragments are gold trimers and the below fragments are silver trimers. CDD maps could clearly reflect the uneven charge distribution in the spatial space and show the electron flow before and after the formation of charge-transfer complexes. Orange regions denote a decrease of electron density while cyan regions denote an increase of electron density versus separated fragments.

REFERENCES

(1) Uson, R.; Laguna, A.; Laguna, M.; Briggs, D. A.; Murray, H. H.; Fackler Jr., J. P. (Tetrahydrothiophene)Gold(I) or Gold(III) Complexes. *Inorg. Synth.* **1989**, *26*, 85-91.

(2) (a) Dias, H. V. R.; Singh, S.; Campana, C. F. Toluene-Sandwiched Trinuclear Copper(I) and Silver(I) Triazolates and Phosphine Adducts of Dinuclear Copper(I) and Silver(I) Triazolates. *Inorg. Chem.* **2008**, *47*, 3943–3945. (b) Dias, H. V. R.; Polach, S. A.; Wang, Z. Coinage Metal Complexes of 3,5-Bis(Trifluoromethyl)Pyrazolate Ligand. *J. Fluor. Chem.* **2000**, *103*, 163–169.

(3) Fujisawa, K.; Ishikawa, Y.; Miyashita, Y.; Okamoto, K.-I. Pyrazolate-Bridged Group 11 Metal(I) Complexes: Substituent Effects on the Supramolecular Structures and Physicochemical Properties. *Inorg. Chim. Acta* **2010**, *363*, 2977–2989.

(4) (a) *Burker APEX2*. Bruker AXS Inc: Madison WI **2007**. (b) *Bruker SAINT*. Bruker AXS Inc: Madison, WI **2007**. (c) *Bruker SADABS*. Bruker AXS Inc: Madison, WI **2007**. (d) Sheldrick, G. M. Crystal Structure Refinement with SHELXL. *Acta Crystallogr., Sect. C: Struct. Chem.* **2015**, *C71*, 3-8. (e) Dolomanov, O. V.; Bourhis, L. J.; Gildea, R. J.; Howard, J. A. K.; Puschmann, H. OLEX2: A Complete Structure Solution, Refinement and Analysis Program. *J. Appl. Cryst.* **2009**, *42*, 339–341.

(5) (a) Kresse, G.; Furthmüller, J. Efficiency of Ab-Initio Total Energy Calculations for Metals and Semiconductors Using A Plane-Wave Basis Set. *Comput. Mater. Sci*. **1996**, *6*, 15–50. (b) Kresse, G.; Joubert, D. From Ultrasoft Pseudopotentials to the Projector Augmented-Wave Method. *Phys. Rev. B* **1999**, *59*, 1758–1775.

(6) Perdew, J. P.; Burke, K.; Ernzerhof, M. Generalized Gradient Approximation Made Simple. *Phys. Rev. Lett.* **1996**, *77*, 3865–3868.

(7) Brothers, E. N.; Izmaylov, A. F.; Normand, J. O.; Barone, V.; Scuseria, G. E. Accurate Solid-State Band Gaps via Screened Hybrid Electronic Structure Calculations. *J. Chem. Phys.* **2008**, *129*, 011102.

(8) Monkhorst, H. J.; Pack, J. D. Special Points for Brillouin-Zone Integrations. *Phys. Rev. B* **1976**, *13*, 5188–5192.

(9) Portmann, S.; Lüthi, H. P. MOLEKEL: An Interactive Molecular Graphics Tool. *Chimia* **2000**, *54*, 766–770.

(10) *Gaussian 16. A. 03*. Frisch, M. J.; Trucks, G. W.; Schlegel, H. B.; Scuseria, G. E.; Robb, M. A.; Cheeseman, J. R.; Scalmani, G.; Barone, V.; Petersson, G. A.; Nakatsuji, H.; Li, X.; Caricato, M.; Marenich, A. V.; Bloino, J.; Janesko, B. G.; Gomperts, R.; Mennucci, B.; Hratchian, H. P.; Ortiz, J. V.; Izmaylov, A. F.; Sonnenberg, J. L.; Williams-Young, D.; Ding, F.; Lipparini, F.; Egidi, F.; Goings, J.; Peng, B.; Petrone, A.; Henderson, T.; Ranasinghe, D.; Zakrzewski, V. G.; Gao, J.; Rega, N.; Zheng, G.; Liang, W.; Hada, M.; Ehara, M.; Toyato, K.; Fukuda, R.; Hasegawa, J.; Ishida, M.; Nakajima, T.; Honda, Y.; Kitao, O.; Nakai, H.; Vreven, T.; Throssell, K.; Montgomery, J. A. Jr.; Peralta, J. E.; Ogliaro, F.; Bearpark, M. J.; Heyd, J. J.; Brothers, E. N.; Kudin, K. N.; Staroverov, V. N.; Keith, T. A.; Kobayashi, R.; Normand, J.; Raghavachari, K.; Rendell, A. P.; Burant, J. C.; Iyengar, S. S.; Tomasi, J.; Cossi, M.; Millam, J. M.; Klene, M.; Adamo, C.; Cammi, R.; Ochterski, J. W.; Martin, R. L.; Morokuma, K.; Farkas, O.; Foresman, J. B.; Fox, D. J. Gaussian, Inc.: Wallingford CT **2016**.

(11) (a) Grimme, S. Semiempirical GGA-Type Density Functional Constructed with A Long-Range Dispersion Correction. *J. Comput. Chem.* **2006**, *27*, 1787–1799. (b) Grimme, S.; Ehrlich, S.; Goerigk, L. Effect of the Damping Function in Dispersion Corrected Density Functional Theory. *J. Comput. Chem.* **2011**, *32*, 1456–1465.

(12) (a) Cundari, T. R.; Stevens, W. J. Effective Core Potential Methods for the Lanthanides. *J. Chem. Phys.* **1993**, *98*, 5555–5565. (b) Stevens, W. J.; Krauss, M.; Basch, H.; Jasien, P. G. Relativistic Compact Effective Potentials and Efficient, Shared-Exponent Basis Sets for the Third-, Fourth-, and Fifth-Row Atoms. *Can. J. Chem.* **1992**, *70*, 612–630.

(13) (a) Zhao Y.; Truhlar, D. G. The M06 Suite of Density Functionals for Main Group Thermochemistry, Thermochemical Kinetics, Noncovalent Interactions, Excited States, and Transition Elements: Two New Functionals and Systematic Testing of Four M06-Class Functionals and 12 Other Functionals. *Theor. Chem. Acc.* **2008**, *120*, 215–241. (b) Zhao Y.; Truhlar, D. G. Density Functionals with Broad Applicability in Chemistry. *Acc. Chem. Res.* **2008**, *41*, 157–167.

(14) (a) Noro, T.; Sekiya, M.; Koga, T. Sapporo-(DKH3)-nZP (N = D, T, Q) Sets for the Sixth Period S-, D-, and P-Block Atoms. *Theor. Chem. Acc.* **2013**, *132*, 1363. (b) Noro, T.; Sekiya, M.; Koga, T. Segmented Contracted Basis Sets for Atoms H Through Xe: Sapporo-(DK)-nZP Sets (N = D, T, Q). *Theor. Chem. Acc.* **2012**, *131*, 1124. (c) Dunning Jr., T. H. Gaussian Basis Sets for Use in Correlated Molecular Calculations. I. the Atoms Boron Through Neon and Hydrogen. *J. Chem. Phys.* **1989**, *90*, 1007–1023.

(15) (a) Lu, T.; Chen, F. Multiwfn: A Multifunctional Wavefunction Analyzer. *J. Comput. Chem.* **2011**, *33*, 580–592. (b) Humphrey, W.; Dalke, A.; Schulten, K. VMD: Visual Molecular Dynamics. *J. Mol. Graphics* **1996**, *14*, 33–38.

(16) (a) Johnson, E. R.; Keinan, S.; Mori-Sánchez, P.; Contreras-García, J.; Cohen, A. J.; Yang, W. Revealing Noncovalent Interactions. *J. Am. Chem. Soc.* **2010**, *132*, 6498–6506. (b) Seifert, N. A.; Hazrah, A. S.; Jäger, W. The 1-Naphthol Dimer and Its Surprising Preference for π–π Stacking Over Hydrogen Bonding. *J. Phys. Chem. Lett.* **2019**, *10*, 2836–2841.

(17) (a) Ziegler, T.; Rauk, A. A Theoretical Study of the Ethylene-Metal Bond in Complexes Between Cu^+, Ag^+, Au^+, Pt^0, or Pt^{2+} and Ethylene, Based on the Hartree-Fock-Slater Transition-State Method. *Inorg. Chem.* **1979**, *18*, 1558–1565. (b) Ziegler, T.; Rauk, A. CO, CS, N_2, PF_3, and $CNCH_3$ as σ Donors and π Acceptors. A Theoretical Study by the Hartree-Fock-Slater Transition-State Method. *Inorg. Chem.* **1979**, *18*, 1755–1759.

(18) *ADF 2018*. SCM, Theoretical Chemistry, Vrije Universiteit, Amsterdam, The Netherlands, https://www.scm.com.

(19) (a) van Lenthe, E.; Baerends, E. J. Optimized Slater-Type Basis Sets for the Elements 1–118. *J. Comput. Chem.* **2003**, *24*, 1142–1156. (b) van Lenthe, E.; Baerends, E. J.; Snijders, J. G. Relativistic Regular Two-Component Hamiltonians. *J. Chem. Phys.* **1993**, *99*, 4597–4610. (c) van Lenthe, E.; Baerends, E. J.; Snijders, J. G. Relativistic Total Energy Using Regular Approximations. *J. Chem. Phys.* **1994**, *101*, 9783–9792.

(20) (A) Lee, C.; Yang, W.; Parr, R. G. Development of the Colle-Salvetti Correlation-Energy Formula into A Functional of the Electron Density. *Phys. Rev. B* **1988**, *37*, 785–789. (b) Becke, A. D. Density-Functional Thermochemistry. III. the Role of Exact Exchange. *J. Chem. Phys.* **1993**, *98*, 5648–5652.

(21) Mitoraj, M. P.; Michalak, A.; Ziegler, T. A Combined Charge and Energy Decomposition Scheme for Bond Analysis. *J. Chem. Theory Comput.* **2009**, *5*, 962–975.

(22) Turney, J. M.; Simmonett, A. C.; Parrish, R. M.; Hohenstein, E. G.; Evangelista, F.; Fermann, J. T.; Mintz, B. J.; Burns, L. A.; Wilke, J. J.; Abrams, M. L.; Russ, N. J.; Leininger, M. L.; Janssen, C. L.; Seidl, E. T.; Allen, W. D.; Schaefer, H. F.; King, R. A.; Valeev, E. F.; Sherrill, C. D.; Crawford, T. D. Psi4: An Open-Source Ab Initio Electronic Structure Program. *WIREs Comput. Mol. Sci.* **2012**, *2*, 556-565.

(23) Parrish, R. M.; Burns, L. A.; Smith, D. G. A.; Simmonett, A. C.; DePrince III, A. E.; Hohenstein, E. G.; Bozkaya, U.; Sokolov, A. Yu.; Di Remigio, R.; Richard, R. M.; Gonthier, J. F.; James, A. M.; McAlexander, H. R.; Kumar, A.; Saitow, M.; Wang, X.; Pritchard, B. P.; Verma, P.; Schaefer III, H. F.; Patkowski, K.; King, R. A.; Valeev, E. F.; Evangelista, F. A.; Turney, J. M.; Crawford, T. D.; Sherrill, C. D. Psi4 1.1: An Open-Source Electronic Structure Program Emphasizing Automation, Advanced Libraries, and Interoperability. *J. Chem. Theory Comput.* **2017**, *13*, 3185–3197.

(24) Jeziorski, B.; Moszynski, R.; Szalewicz, K. Perturbation Theory Approach to Intermolecular Potential Energy Surfaces of van der Waals Complexes. *Chem. Rev.* **1994**, *94*, 1887-1930.

(25) Hohenstein, E. G.; Parrish, R. M.; Sherrill, C. D.; Turney, J. M.; Schaefer, H. F. Large-scale Symmetry-Adapted Perturbation Theory Computations via Density Fitting and Laplace Transformation Techniques: Investigating the Fundamental Forces of DNA-Intercalator Interactions. *J. Chem. Phys.* **2011**, *135*, 174017.

(26) Hohenstein, E. G.; Sherrill, C. D. Density Fitting and Cholesky Decomposition Approximations in Symmetry-Adapted Perturbation Theory: Implementation and Application to Probe the Nature of π−π Interactions in Linear Acenes. *J. Chem. Phys.* **2010**, *132*, 184111.

(27) Parker, T. M.; Burns, L. A.; Parrish, R. M.; Ryno, A. G.; Sherrill, C. D. Levels of Symmetry Adapted Perturbation Theory (SAPT). I. Efficiency and Performance for Interaction Energies. *J. Chem. Phys.* **2014**, *140,* 094106.

(28) (a) Weigend, F.; Ahlrichs, R. Balanced Basis Sets of Split Valence, Triple Zeta Valence and Quadruple Zeta Valence Quality for H to Rn: Design and assessment of accuracy. *Phys. Chem. Chem. Phys*. **2005**, *7*, 3297-3305. (b) Andrae, D.; Häußermann, U.; Dolg, M.; Stoll, H.; Preuß, H. Energy-Adjusted Ab Initio Pseudopotentials for the Second and Third Row Transition Elements. *Theor. Chim. Acta* **1990**, *77*, 123-141.

(29) Galassi, R.; Ghimire, M. M.; Otten, B. M.; Ricci, S.; McDougald, R. N., Jr.; Almotawa, R. M.; Alhmoud, D.; Ivy, J. F.; Rawashdeh, A.-M. M.; Nesterov, V. N.; Reinheimer, E. W.; Daniels, L. M.; Burini, A.; Omary, M. A. Cupriphication of Gold to Sensitize d^{10}–d^{10} Metal–Metal Bonds and Near-Unity Phosphorescence Quantum Yields. *Proc. Natl. Acad. Sci. U.S.A.* **2017**, *114*, E5042–E5051.

(30) Mohamed, A. A.; Galassi, R.; Papa, F.; Burini, A.; Fackler, J. P., Jr. Gold(I) and Silver(I) Mixed-Metal Trinuclear Complexes: Dimeric Products From the Reaction of Gold(I) Carbeniates or Benzylimidazolates with Silver(I) 3,5-Diphenylpyrazolate. *Inorg. Chem.* **2006**, *45*, 7770–7776.

(31) Mohamed, A. A.; Burini, A.; Fackler, J. P., Jr. Mixed-Metal Triangular Trinuclear Complexes: Dimers of Gold−Silver Mixed-Metal Complexes From Gold(I) Carbeniates and Silver(I) 3,5-Diphenylpyrazolates. *J. Am. Chem. Soc.* **2005**, *127*, 5012–5013.